Time-resolved electron microscopy by means of electron counting

Nobuyuki Osakabe
Advanced Research Laboratory, Hitachi, Ltd., Hatoyama, Saitama 350-03, Japan

Tetsuji Kodama
Department of Information Electronics, Nagoya University, Nagoya 464-01, Japan

Akira Tonomura
Advanced Research Laboratory, Hitachi, Ltd., Hatoyama, Saitama 350-03, Japan
(Received 19 February 1997)

A method of time-resolved electron microscopy has been developed and applied to the study of the vortex-line dynamics in a type-II superconductor and to the measurement of the elastic properties of nanoscaled materials. Exploiting an electron counting technique, time-dependent electron microscope image beam current, position selected by a probing aperture in the image plane, is measured as sequentially sampled electron counts or a temporal and spatial correlation function which can be converted to the spectral density function. Experimental techniques of detectors and correlators, presently allowing the measurement of the correlation function up to the GHz range, are described. Fundamental electron counting statistics for the measurement of a counting distribution, a power spectral density, and a cross-correlation function are examined using uncorrelated electrons in a beam from a field-emission source. The intrinsic electron correlation due to the second-order coherence appearing in the quest for fast time-resolved observation is also discussed with regard to its offering possibilities of interferometric measurements. [S0163-1829(97)01634-2]

I. INTRODUCTION

The objective of condensed matter physics is to describe the physical properties of matter from the microscopic point of view in the most general way possible. Electron microscopy (EM) has been used to obtain atomic-scale structural information, which gives the starting point for the description of matter, but EM image observation gives us only limited access to the individual or collective dynamics of electrons and atoms. The most widely used previous approach was to follow each event in real time (*in situ* observation). The temporal resolution is then in principle determined by the statistical fluctuations of electrons forming an image. This means that when the duration of the image acquisition is short ($\leqslant$ms), the signal-to-noise ratio is low.

To overcome this limitation, stroboscopic techniques were first introduced in mirror electron microscopy.[1] Scanning electron microscopy (SEM) using those techniques has been used to observe the signal propagation in electric devices:[2] a short-pulse electron beam (pulse widths $\leqslant$ps are available)[3] synchronized to the period of the device's operation is used to observe a phase of the operation period as a still image. The pulse-beam techniques are also used in transmission electron microscopy (TEM)[4] and in reflection high-energy electron diffraction (RHEED).[5] This approach, however, is limited to the observation of highly periodic phenomena or of events for which the trigger signals are available, and this is often not the case when we are concerned with the dynamics of the constituents of matter.

Another method of time-resolved observation in EM images has, therefore, been devised.[6,7] An imaging electron beam current, temporally modulated by the dynamics of the specimen, is selected by the aperture in the image plane and is sampled by means of an electron counting technique.[8] Two-dimensional information can be obtained by using an array of detectors or by scanning the image, and in this context the present method can be called time-resolved electron microscopy.

Bostanjoglo and Liedke[9] measured a time-dependent TEM image beam current in order to observe melting of a crystal by using a scintillator and a photomultiplier tube. This current measurement in analog mode used a large current ($\approx$10 nA), and a wide area ($\approx \mu m^2$) had to be monitored.

The present method exploits electron counting techniques, so an extremely small current ($\leqslant$ fA) can be monitored and the data is accumulated to reduce the statistical error of an appropriate function characterizing the time dependence of the current. Sequentially sampled (with a variable sampling interval) electron counts can be used to follow events directly if the image contrast (i.e., modulation of the beam current) is statistically significant. Faster phenomena can be observed as a temporal and spatial correlation function obtained by the sequential sampling and the numerical computation or by a correlator based on a coincidence-delay measurement.[10] The dynamics of an ensemble of elements are often formulated as the correlation function, rather than as the motion of the individual elements, so the results are easily compared with those predicted by a theoretical treatment. The technical basis for this method consists of fast-response electron detectors and fast logic circuits, and a correlator working with a frequency of up to the GHz range has already been achieved.[8]

In this article, the method and its application are described with the fundamental electron counting statistics examined. We also mention that the quest for fast time-resolved obser-

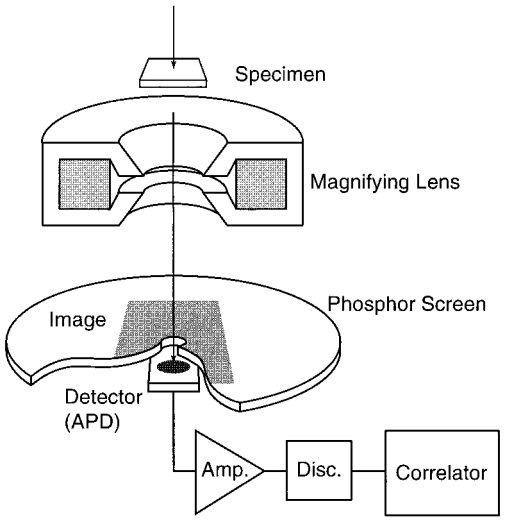

FIG. 1. Method of time-resolved electron microscopy with a single detector.

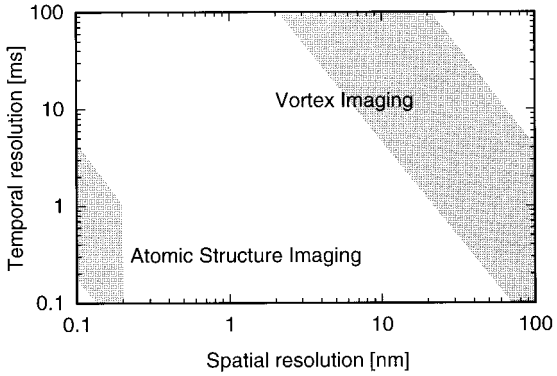

FIG. 2. Temporal resolution of the TEM observation as a function of the spatial resolution. Atomic structure imaging is assumed to be done with the beam divergence angle β between 5×10^{-4} and 1×10^{-3} rad. Vortex observation by Lorentz microscopy is assumed to be done with $10^{-7}<\beta<10^{-6}$. Brightness of 1×10^{9} A/cm^2 is assumed.

vation will be confronted by the intrinsic electron correlation in a coherent beam due to the particle exchange antisymmetry.[11]

II. EXPERIMENTAL

A. Configuration

The present time-resolved observation can be done without major modification of a standard TEM. Figure 1 shows a simple embodiment of the time-resolved electron microscopy. An image of the specimen is magnified through the electron lenses (only a single lens is shown) and projected onto the phosphor screen in the observation chamber. The detector can be installed behind the screen. The output signals are led to a preamplifier and a discriminator that make it possible to count each electron without error.

There are several ways of to sample the data and to configure the detector. The data sampling methods are (1) sequential sampling of the number of counts with variable interval and (2) correlation function measurement by means of a coincidence-delay technique.

Sequential counts can be used to follow the event directly. The resolving time can be defined[12] as the minimum width of the sampling interval T in which the object is detectable with a given signal-to-noise ratio N_σ: $K\sqrt{\overline{n}}\geq N_\sigma$, where K is the visibility of the object, and $\overline{n}$ is the average count in the sampling interval ($\overline{n}=\pi r_0^2 iT/e$, where i is the current density, r_0 is the radius of the probing aperture, and e is the electron charge). This $\overline{n}$ is constrained by the invariance[13] of the brightness $B=i/\pi\beta^2$ (β is the beam divergence half angle), since an EM observation requires a certain transversal coherence length $\approx\lambda/2\beta$ (λ is the wavelength). Then the minimum resolvable time is given as

$$T_{\min}=\frac{e}{B}\left(\frac{N_\sigma}{\pi r_0\beta K}\right)^2. \tag{1}$$

The relation in Eq. (1) is shown in Fig. 2 for the observation of atomic structure images in high-resolution transmission electron microscopy (HRTEM) and for the magnetic-vortex images in Lorentz microscopy.[14] In the case of HRTEM, a required value of β is determined from the envelope of the contrast transfer function.[15] In Lorentz electron microscopy, β should be smaller than the beam deflection at the magnetic field of a vortex.[16] A brightness[17] of 1×10^9 A/cm^2 is assumed. Approximately 1 ms is the minimum resolvable time for both atom dynamics and vortex dynamics observations. Faster phenomena can be evaluated by numerically calculating the spectral density or the correlation function from the sequentially sampled data, but this requires a large amount of memory (depending on the duration of the measurement) and the data transfer to memory is time-consuming.

A coincidence-delay measurement with electric shift-registers as delays gives the correlation function in a more elegant manner. A digital correlator working with the clock frequency up to the GHz range can be constructed using electric circuit and detector technology (Secs. II B and II C). Since the error of the counting data is given by the statistical fluctuation, a given signal-to-noise ratio is achieved by the data acquisition of appropriate duration (details of statistical relation are discussed in Sec. III). The spectral density can be found by calculating the Fourier transform of the correlation function.

Single, double, and multiple detectors can be used. With a single detector, autocorrelation and power spectral density can be obtained, and a two-dimensional map of those functions can be derived by scanning the image.

When we have two detectors, the cross correlation function can be observed. The temporal and spatial correlation map can be obtained by changing the sites of the detectors or by using the electron biprism,[18] which is usually used to overlap two electron waves to make interference measurements.[19] Two electron biprisms perpendicular to each other may be used to locate any two positions in the image at the fixed two detector positions. This may be useful in the observation of the correlation function of the vortex transports.

A multiple-detector configuration would make the abovementioned measurement easier by allowing parallel processing to obtain complete spatial and temporal correlation func-

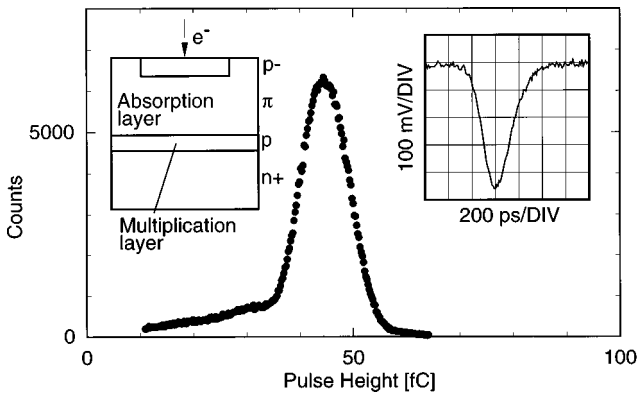

FIG. 3. Pulse height distribution of a Si-APD for 50-keV electrons. Left inset: schematic structure of the Si-APD. Right inset: wave form of the output pulse.

tion. The technical difficulties of the multiple-detector configuration are due to the possible cross-talk between adjacent detector elements.

B. Detectors

There are several choices of detector: (1) scintillators and photomultipliers, (2) microchannel plates (MCP's), (3) photodiodes (PD's), and (4) avalanche photodiodes (APD's). The present method requires detectors with a small sensitive area and a fast response with a small dead time. The APD is thus an ideal detector for this application.

A schematic of the structure of a Si-APD is shown in the left inset of Fig. 3. Electrons incident on the APD deposit the energy to generate electron-hole pairs (3.61 eV/pair)[10] in the absorption layer. The electrons are injected into the multiplication layer, where the successive impact ionization by the accelerated carriers in the electric field multiply the charges, giving low-noise amplification.[20] This internal gain plays an important role, especially in a fast circuit ($\geqslant$ GHz), in pulling signals from the noise level, because the noise figure of the avalanche amplification is smaller than that of the amplifiers based on the electric circuit.

The pulse height distribution (PHD) depends on the primary electron energy and the thickness of the absorption layer.[21] Shown in Fig. 3 is the PHD of a Si-APD (Hamamatsu SPL2941), with a 20-μm-thick absorption layer, for 50-keV electrons.[8] The incident energy is fully absorbed in the absorption layer, giving a sharp distribution. APD's can also be used for electrons of higher energy, in which case the primary electron penetrates the absorption layer to partially deposit its energy.[22]

The wave form of the output pulse is shown in the right inset of Fig. 3. The rise time is 180 ps and the pulse width is 430 ps, allowing a time jitter of $\approx$20 ps in acquiring the arrival timing information[8] and the small dead time determined by the overlapping of two pulses.[10]

C. Correlator

The temporal resolution of the intensity correlation measurement depends on the statistical error reduction by the data accumulation, so an efficient measurement technique is required. A digital correlator based on the coincidence-delay measurement with electric shift registers as delays[23] can be used for this purpose.

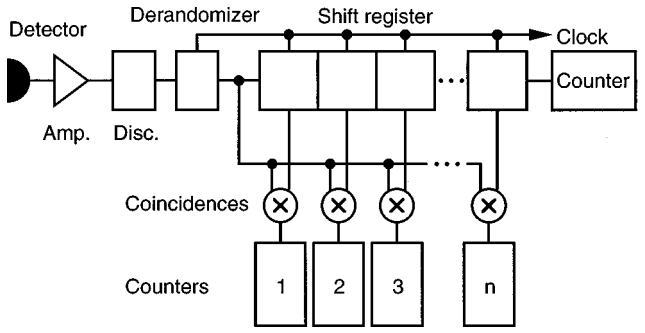

FIG. 4. Block diagram of the autocorrelator. The derandomizer is a circuit where the asynchronous signals are injected into the synchronized circuit.

A diagram of the digital autocorrelator is shown in Fig. 4. Electrons incident on the detector are amplified and then standardized in a discriminator to give a train of pulses corresponding to the temporal distribution of electrons in a beam. The signal is led to the synchronized circuits (''derandomized'')[24] and is moved sequentially down a shift register by a clock of the frequency f_c which determines the sampling interval $T=1/f_c$. It is then cross correlated with the original digital signal by coincidence circuits. The total counts and the coincidence counts are stored to give a normalized autocorrelation $\langle n(t)n(t+ST)\rangle/\langle n(t)\rangle^2$ at $\tau=ST$; n is an electron number current and S is an integer corresponding to the Sth delay channel of the coincidence counts storage. For the work described here, the average electron beam intensity $\overline{n}$ should be sufficiently low that $f_c \gg \overline{n}$. Therefore the slow measurement is better to be done with the sequential sampling and the numerical calculation. The technique described here can be easily extended to the cross correlator.

A digital correlator with clock frequency of about 100 MHz and with about 10^3 delay channels can be designed with versatile field programmable gate arrays (FPGA's). A 5-GHz digital cross correlator with five delay channels has already been made.[8] To make a GHz correlator with an acceptable number of delay channels, problems of low-skew clock distribution and the power consumption should be solved. We also note that the recent progress of data acquisition and analysis in high-energy physics[25] and the advance in the lightwave communication systems[26] may provide the technology for fast detectors as well as an appropriate way of handling data.

III. COUNTING STATISTICS

Electron counting statistics relevant to the error estimation are examined with an electron beam and without a specimen. When a current consisting of uncorrelated electrons is measured as the sequential counts of electrons, the distribution is known to be a Poissonian represented by the probability density to count n electrons in a sampling interval T, $P_n(T)=(\alpha T)^n \exp(-\alpha T)/n!$ (α is the counting rate). The standard deviation is given by $\sigma=\sqrt{n}$. Shown in Fig. 5 is the distribution of field-emitted electrons sampled with

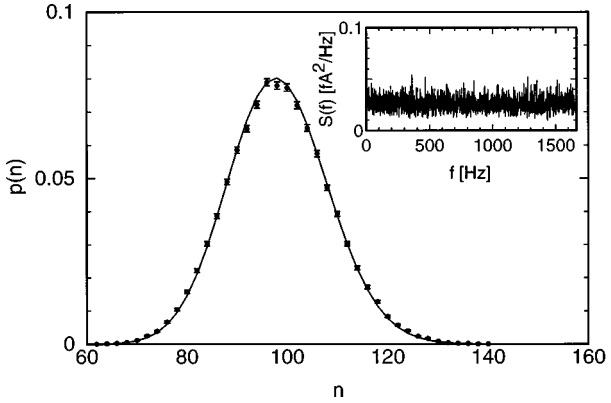

FIG. 5. Electron counting distribution. Electron counts in 200 μs at intervals of 300 μs were taken over 65 536 sampling points with a 300-keV field emission electron microscope. The Poisson distribution is shown by the line connecting the points. Inset: power spectral density. Power spectral density were Fourier transformed from the sampled data with averaging successive 16 points.

$T=200$ μs and $\alpha=4.91\times10^5$ counts/s. The distribution is almost consistent with the Poissonian, but is slightly wider (''super-Poisson''). This is also shown by $\sigma^2=104$ larger than $\overline{n}=98.3$. This widening is due to the field-emission noise described in Sec. IV. The detailed test of the distribution of uncorrelated electrons should be done with a higher sampling frequency.[27]

The cross correlation function $C_{12}(\tau)$ can be defined as

$$C_{12}(\tau)=\langle I(\mathbf{r}_1,t)I(\mathbf{r}_2,t+\tau)\rangle, \tag{2}$$

where $I(\mathbf{r}_i,t)$ is an electron beam current at a position $\mathbf{r}_i$ and a time t. The normalized cross-correlation function $R_{12}(\tau)$ is defined as $C_{12}(\tau)/\langle I(\mathbf{r}_1,t)\rangle\langle I(\mathbf{r}_2,t)\rangle$. The raw cross-correlation function $C_{12}(\tau)$ is related to the (one-sided) cross-spectral density $S_{12}(\omega)$ as

$$S_{12}(\omega)=2\int_{-\infty}^{\infty}C_{12}(\tau)e^{i\omega\tau}d\tau. \tag{3}$$

If electrons in the current are uncorrelated, or following the Poisson process, $R_{12}(\tau)=1$ and the power spectral density $S_{11}(\omega)=2e\langle I(\mathbf{r}_1,t)\rangle$.[28] Shown in the inset in Fig. 5 is a power spectral density of the current. It is white spectral density and the average value of 0.0260 fA^2/Hz is consistent with the value $2e\overline{I}=0.0252$ fA^2/Hz ($\overline{I}=78.7$ fA). Again the slight discrepancy is a result of the additional fluctuations due to field-emission noise.

Measurement of the current and the correlation function by using electron counting technique will be done in the finite duration of the total sampling time T_s and finite sampling interval T. Using the correlator shown in Fig. 4, the normalized cross-correlation function is obtained as

$$R_{12}(\tau_i)=\frac{(1/M)\sum_{j=1}^{M}n_{12}(\tau_i,t_j)}{(1/M^2)\sum_{j=1}^{M}n_1(t_j)\sum_{j=1}^{M}n_2(t_j)}, \tag{4}$$

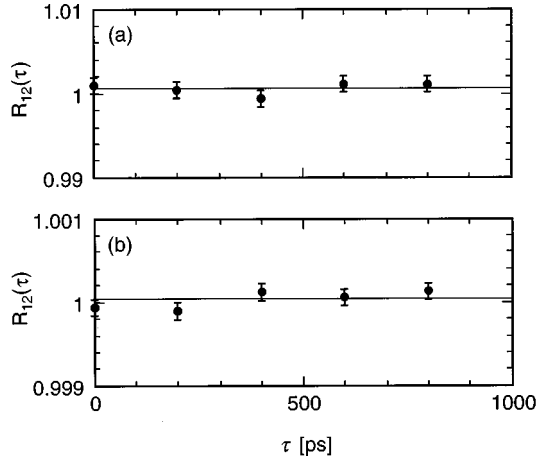

FIG. 6. Cross-correlation function of uncorrelated electrons: (a) $\sigma=0.97\times10^{-3}$; (b) $\sigma=1.0\times10^{-4}$.

where $M=T_s/T$ is the number of samplings, $n_k(t_j)$ is the numbers of counts of the kth detector in the jth time bin, and $n_{12}(\tau_i,t_j)$ is the number of coincidence counts of the ith time delay in the jth time bin. The interval of the delay and the duration of the sampling are both T. The statistical error in the estimation of the normalized cross-correlation function is given by

$$\frac{\delta R_{12}}{R_{12}}=\frac{\sqrt{1+\overline{n_1}+\overline{n_2}}}{\sqrt{M\overline{n_1}\,\overline{n_2}}}. \tag{5}$$

Figure 6 shows the normalized cross correlation of field-emitted electrons taken with a digital correlator working at a clock frequency of 5 GHz. The counting rate was $\approx1\times10^7$ counts/s for both detectors. Total sampling time was ≈50 s for (a) and ≈5000 s for (b). Statistical errors determined by Eq. (5) are shown as bars in the figure. The cross-correlation function is consistent with the statistical predictions for uncorrelated electrons, constant ($=1$) over the measured delay of 800 ps.

IV. INTRINSIC FLUCTUATIONS

A. Field-emission noise

Field-emission current has been known to exhibit a fluctuation other than the shot noise.[29] This fluctuation is due to the hopping of the absorbed residual gas molecules changing the work function of the emitter surface. The lifetime of the hopping interval is $\approx$ ms. Amplitude of the fluctuation is $\approx10\%$ of the current. The power spectral density of the beam current was experimentally found[29] as $S(\omega)\propto f^{-\epsilon}$, $(0.8<\epsilon<1.3)$, giving a rapid decay in the high-frequency region. This fluctuation does not seriously affect the measurement faster than a millisecond.

B. Two-electron interference

If a coherent electron beam is used, two-electron interference occurs and $R_{12}(\tau)$ exhibits the anticorrelation due to the particle (fermion) exchange symmetry.[11] Silverman[30] derived the correlation function

$$R_{12}(\tau)=1-\kappa_{12}(\tau), \tag{6}$$

where $\kappa_{12}(\tau)$ is given by

$$\kappa_{12}=\frac{\epsilon}{\Sigma_1\Sigma_2}\int_{\Sigma_1} d\mathbf{r}_1 dt_1 \int_{\Sigma_2} d\mathbf{r}_2 dt_2 |\gamma(\mathbf{r}_2-\mathbf{r}_1;t_2-t_1)|^2 \tag{7}$$

and ϵ is a factor depending on the polarization of the electron beam giving unity for the fully polarized beam and 1/2 for the unpolarized beam. The term $\Sigma_i(i=1,2)$ denotes the product of the sensitive area of the detector and the coincidence time window, and γ is the first-order degree of coherence[31] written as

$$\gamma=\frac{\int d^3\mathbf{k}k_x n(\mathbf{k})\exp[i\{\mathbf{k}\cdot(\mathbf{r}_2-\mathbf{r}_1)-\omega(t_2-t_1)\}]}{\int d^3\mathbf{k}k_x n(\mathbf{k})}, \tag{8}$$

where the propagation direction is taken as x and $n(\mathbf{k})$ is a momentum distribution with $\mathbf{k}$ the wave number vector. The dispersion relation is $\omega=\hbar k^2/2m$ with $\hbar$ the Planck's constant and m the elctron mass. This degree of coherence has a significant value within the transversal coherence length $l_t=1/\Delta k_t$ (Δk_t is the transversal wave number spread) and the coherence time $\tau_c=\hbar/\Delta E$ (ΔE is the energy spread). Therefore the correlation function shows the substantial reduction of the probability of finding two particles within the coherence volume ($l_t^2\tau_c v$; v is the average velocity). This is also called ''antibunching,'' in contrast to photon ''bunching'' of the chaotic ensemble.[32] This antibunching is a direct consequence of the Pauli exclusion principle, or the exchange antisymmetry of fermions.

In the field-emission electron beam, the coherence time is $\hbar/\Delta E\approx 2$ fs when $\Delta E=0.4$ eV. This time range is several orders of magnitude shorter than the attainable resolution of the measurement system, but the effect may appear in the correlation function as a small dip $\approx\tau_c/T$ at delay $\tau=0$.[33]

This correlation has not yet been observed, but the two-electron interference could provide not only tests of quantum mechanics[34] but also a way to measure the energy dispersion precisely, since the coherence time measured in the electron correlation is the reciprocal of the energy spread. This is a counterpart of photon correlation spectroscopy.[23]

V. APPLICATIONS

A. Vortex-line dynamics

When a magnetic field is applied to a type-II superconductor, it penetrates the sample in localized tubes of quantized magnetic flux of $h/2e$, which are also known as vortices. Transport currents force the vortices to move and dissipate energy, giving the material a nonzero resistance. Thus it is important to understand the motion of vortices interacting with the pinning potentials.

Lorentz microscopy observation[14] has been used to study the interaction between vortices and the pinning sites[35] by using a 30-frame/s camera. A Lorentz micrograph of a Nb thin film, taken with a 300-keV field emission TEM equipped with a specimen cooling stage, is shown in Fig. 7. The specimen foil was mounted at 45° to the electron beam, and the magnetic field was applied transversally. Individual vortices manifest themselves as tiny globules, one side bright, the other side dark, and the separation line parallel to the vortex line on the image plane.[36] The image contrast can be explained as a consequence of Lorentz deflection of the electron beam by the transverse component of the magnetic flux of vortex-lines: the bright side is formed by the superposition of deflected and transmitted beams, and the dark side is formed by the releasing of the deflected beam.

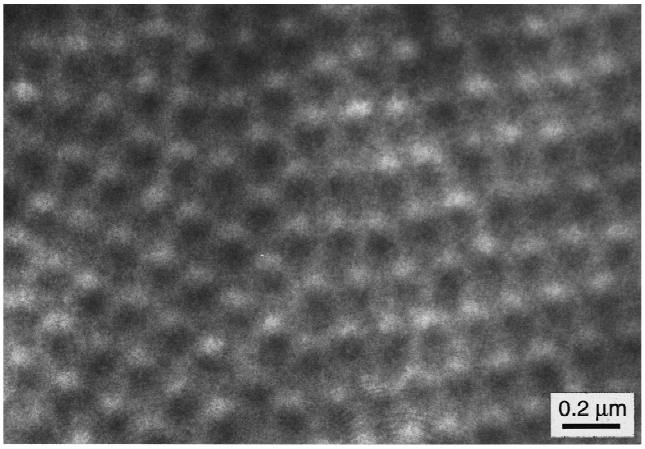

FIG. 7. Lorentz electron micrograph of the vortex-line lattice in a Nb thin film at $T=7.5$ K and $H=75$ G.

The vortices in Fig. 7 are arranged periodically to form the Abrikosov lattice. When the magnetic field applied to the Nb thin film is changed, the vortices relax to a stable configuration by successive hopping.[14] The vortices stayed for a while at particular sites, which are supposed to be pinning sites. Figure 8 shows the sequentially sampled beam current obtained when the probing aperture was set at one of the sites. The image magnification was 2200 and the diameter of the probing aperture corresponded to 90 nm. The counts are represented as the number of electrons detected in 2 ms. The average count is 117 ($\sigma\approx 11$). The high-current states ($\approx$148 counts) beginning at time $\approx$2 s and $\approx$10 s correspond to the vortices staying at the site for about a second.

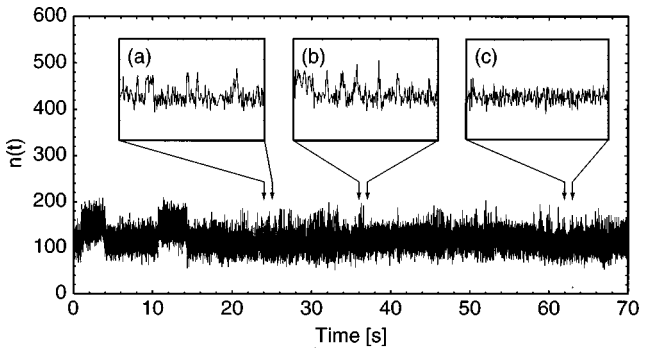

FIG. 8. Sequentially sampled electron counts obtained at intervals of 2 ms. The insets (a)–(c) are enlarged plots with a time span of 500 ms and a vertical span of 250 counts.

The insets show enlarged parts (500 ms) of the current. The narrow peaks in the insets (a) and (b) indicate the vortices staying at the site for ~ms. The inset (c) shows a period when no vortex stayed at the site. The fluctuation of the current in this period is consistent with σ. This type of measurement allows the lifetime of the vortex at the site to be determined, and thus the activation energy to be obtained.[6]

The visibility $[=2|I_{\max}-I_{\min}|/(I_{\max}+I_{\min})]$ of the vortex is ≈ 0.24 and $\sigma/\bar{n}=0.093$ giving a signal-to-noise ratio of 2.6. Thus the sampling interval of 2 ms is almost the limit for this direct tracing of vortices under the conditions used in this observation.

Averaging in time domain is, therefore, needed to access faster phenomena. The measurement of the correlation function is suitable for the study of the dynamics of vortex flow driven by currents.[37] This issue is relevant to the other systems in condensed matter, such as to the dynamics of charge density waves,[38] and has thus been attracting considerable interest over the past few years. One experimental approach has been through voltage or magnetic flux noise measurements[39] characterizing the collective motion of vortices. The present method provides the vortex density correlation function directly.

The objective of this kind of experiment is to find how the vortex lines are arranged when driven by the current. This arrangement is formulated[39] by the vortex density correlation function $R_v(\mathbf{r}_1,\mathbf{r}_2,\tau)$:

$$R_v(\mathbf{r}_1,\mathbf{r}_2,\tau)=\langle\rho(\mathbf{r}_1,t)\rho(\mathbf{r}_2,t+\tau)\rangle, \tag{9}$$

$$\rho(\mathbf{r},t)=\sum_i \delta^{(2)}[\mathbf{r}-\mathbf{r}_i(t)]. \tag{10}$$

Here $\rho(\mathbf{r},t)$ denotes the vortex density function consisting of a set of two-dimensional delta functions $\delta^{(2)}$. An image beam current is given as

$$I(\mathbf{r},t)=I_0\int[1+\rho(\mathbf{r}',t)*K(\mathbf{r}')]dS. \tag{11}$$

Here the asterisk denotes a convolution, I_0 is an average current, and $K(\mathbf{r})$ is an image intensity function of a vortex.[36] The integration should be performed in the probing aperture area. Thus, the correlation function of the image beam current essentially represents the vortex density correlation function.

The elastic flow of vortices was simulated by feeding a triangular wave current to the image shift coils in order to make the Lorentz image oscillate. The specimen was a Nb film cooled to 7.5 K and under a magnetic field of 75 G. The image was oscillated by about ≈ 1.7 μm, corresponding to about three vortex intervals, with a frequency of 1 Hz. The inset in Fig. 9(a) shows the sequential counts obtained with the sampling interval of 5 ms. The oscillation corresponds to the bright and dark part of vortex image passing the probing aperture. 6-Hz oscillation is clearly evident in the normalized autocorrelation is shown in Fig. 9(a). If we assume that the

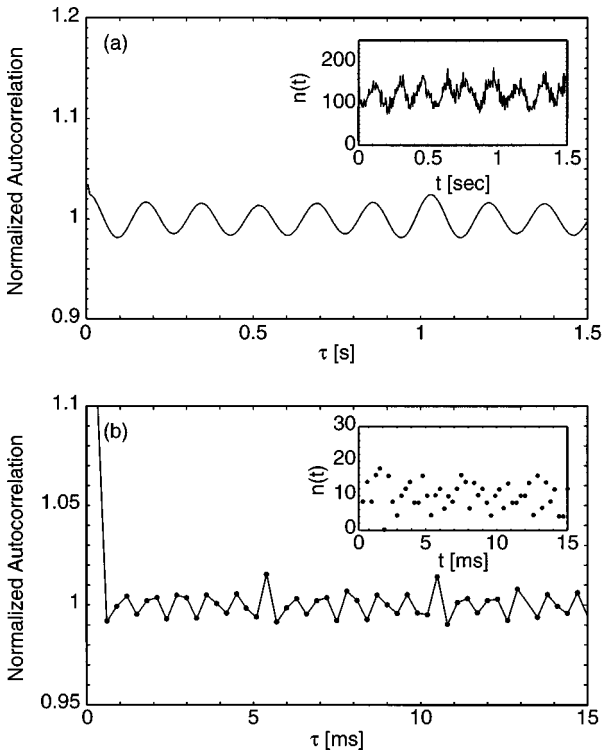

FIG. 9. Autocorrelation functions of an oscillated vortex-line lattice image obtained with a Nb film at 7.5 K and 75 G, simulating elastic vortex flow. The image was oscillated with an amlitude of about three vortex intervals at triangular wave frequencies of (a) 1 Hz and (b) 200 Hz. Lines are drawn to guide eyes.

time-dependent current I is sinusoidal as $I=I_0(1+a\cos\omega t)$, with $2a$ the visibility of vortices and I_0 the average current, the normalized autocorrelation function $R(\tau)=1+1/2a^2\cos\omega t$. The amplitude in the autocorrelation function ≈ 0.016 is consistent with the visibility ≈ 0.37 found in the sequentially sampled counts.

The faster scan is shown in Fig. 9(b). The amplitude of the image oscillation is same, but the frequency is 200 Hz. The average count in the 300-μs sampling intervals is 10.4, so the sequential counts do not show statistically significant information. The autocorrelation measured for 13 s clearly shows the oscillation with frequency ≈ 1.2 kHz. Large peaks at $\tau\approx 5$ ms and $\tau\approx 10$ ms in the cross correlation are due to the 200-Hz true frequency. In this case the amplitude in the normalized autocorrelation is ≈ 0.01, smaller than the value in (a). This is because the frequency of 1.2 kHz is close to the 1.6-kHz sampling limit under these conditions. These measurements were done with the sequential sampling and the numerical calculation. The sampling frequency and the length of the total sampling time in (b) represents the maximum performance of the present apparatus. The correlator described in Sec. II will provide the correlation function up to 100 MHz without constraint on the total sampling time. Thus the feasibility of observing the elastic flow depends on the total sampling time needed to achieve the acceptable signal-to-noise ratio, whose time is given by the statistical error Eq. (5) and the amplitude of the correlation function mentioned above.

B. Vibration analysis

Recently mechanical properties of nanoscale materials, especially fullerenes and their relatives, have attracted interest because of their potential practical applications.[40] The evaluation of the elastic properties by means of the conventional method[41] has been difficult, however, because of the small sample sizes. Recent work by Treacy, Ebbesen, and Gibson[42] measured the temperature-dependent amplitude of the thermal vibration of carbon nanotubes as a blurring of the electron microscope images in order to estimate the Young's modulus of the tubes. Elastic constants can be found from the effective spring constant k of the specimen. The average elastic energy $1/2ku^2$ (u is the vibration amplitude) is, from the principle of equipartition, equal to $1/2k_BT$, with k_B being Boltzmann's constant and T the absolute temperature. Consequently, the measured $\langle u^2 \rangle$ gives the spring constant.

Time-resolved electron microscopy can be used to find the resonance frequency of oscillations driven by thermal agitation[7] or damping oscillation initiated by an external force. In the case of thermally driven oscillation, the spring constant and the Q factor have been shown to be found by the power spectral density measurement.[7]

When oscillations are measured using TEM, the effect of the electron beam is crucial. The primary electrons hitting the sample generate the secondary electrons, thus charging the specimen. This charging effect is negligible when conductive materials are used, but materials with low conductivity or contaminated conductive material keep the charge, yielding extra electrostatic force. The resonant frequency is shifted by the presence of the gradient of the force (this is the principle of magnetic force microscopy).[43] The frequency shift is given by

$$\Delta f_0 = \frac{f_0}{2k} \frac{\partial^2 V(y)}{\partial y^2}, \tag{12}$$

where f_0 is the resonant frequency, $V(y)$ is the potential, y is the direction of the oscillation, and k is the spring constant.

Figure 10 shows, for two different primary current densities at the specimen, the power spectral densities of an electron beam current monitoring thermally driven oscillations of a thin Pt wire. If charging up of the specimen introduces an appreciable force gradient on the Pt wire, the resonant frequency should be shifted. We can see in this figure that the use of the primary current densities differing by an order of magnitude does not change the resonant frequency within the resolvable bandwidth of 0.10 Hz. The electrostatic force is considered to be negligible in this case.

VI. CONCLUSION

A method of time-resolved electron microscopy has been described. Time-dependent electron microscope image beam current, position selected by the aperture in the image plane is measured as sequentially sampled electron counts or a correlation function using an electron counting technique.

The error in the counting data is due only to the statistical fluctuations of the number of electrons, so the error reduction resulting from the data accumulation—hence the resolving time in the correlation measurement—depends on whether or not the duration of the total sampling time needed in order to achieve an acceptable signal-to-noise ratio is permissible. Experimental techniques for the detector and the correlator are given, and a correlator working at a frequency up to the GHz range has already been made.

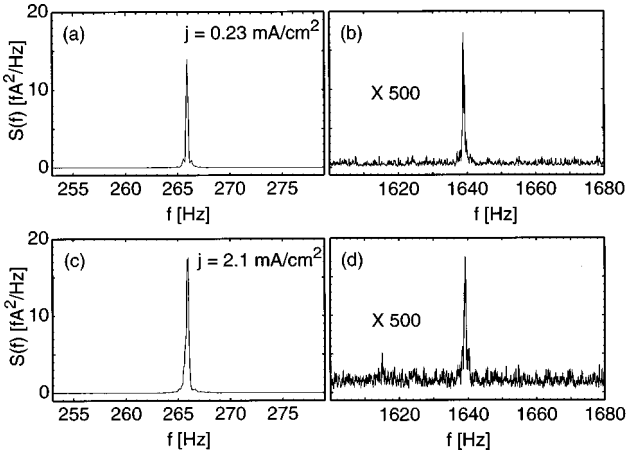

FIG. 10. Power spectral densities of electron beam currents monitoring thermally driven oscillations of a Pt thin wire. (a) and (b) show the fundamental frequency and the first overtone observed when the electron current density was 0.23 mA/cm^2; (c) and (d) show those observed when the electron current density was 2.1 mA/cm^2.

Fundamental electron counting statistics has also been examined by measuring the counting distribution, power spectral density, and cross correlation of uncorrelated electrons in the beam from a field-emission source. This kind of microscopy has so far been used to study vortex-line dynamics and to measure the elastic properties of materials.

The intrinsic electron intensity fluctuations due to the particle exchange antisymmetry has also been described. They have not yet been detected, but their existence opens possibilities for measurement.

In summary, the present method has a growing technical basis and can be applied widely in TEM observation without major modification of the microscopes. The quest for faster observation will be confronted by the intrinsic electron fluctuations, a problem of great interest,[44] but so far experimentally untouched. The progress in experimental technology is giving us the chance to attack this problem.

ACKNOWLEDGMENTS

This work was partially supported by the Japan Science and Technology Corporation. The authors would like to thank H. Kasai, K. Harada, and M. I. Lutwyche of Hitachi, Ltd., for their cooperation with the experiments. Technical supports from S. Kubota, S. Matsunami, and M. Moriya of Hitachi, Ltd., are gratefully acknowledged. The authors acknowledge J. Endo of Hitachi, Ltd., T. Urakami, S. Ohsuka, K. Tsuchiya, and Y. Tsuchiya of Hamamatsu Photonics, and K. Ohbayashi of Kowa Company, Ltd., for their cooperation in the development of the APD's and the correlator. Discussions with S. Asai of Hitachi, Ltd., contributed significantly to this study and are gratefully acknowledged.

[1] A. E. Lukianov and G. V. Spivak, in *Proceedings of 6th International Congress for Electron Microscopy, Kyoto, 1966* (Maruzen, Tokyo, 1966), p. 611.
[2] G. S. Plows and W. C. Nixon, J. Phys. E **1**, 595 (1968).
[3] T. Hosokawa, F. Fujioka, and K. Ura, Rev. Sci. Instrum. **49**, 624 (1978).
[4] O. Bostanjoglo and Th. Rosin, in *Proceedings of the 7th European Congress on Electron Microscopy, Hague, 1980* (7th European Congress on Electron Microscopy Foundation, Leiden, 1980), Vol. 1, p. 88; O. Bostanjoglo and Th. Rosin, Phys. Status Solidi A **57**, 561 (1980); K. Ura, H. Fujioka, T. Saito, and N. Morimura, J. Electron Microsc. **27**, 311 (1978); A. Takaoka and K. Ura, *ibid.* **32**, 299 (1983).
[5] H. E. Elsayed-Ali and J. W. Herman, Appl. Phys. Lett. **57**, 1508 (1990); J. W. Herman and H. E. Elsayed-Ali, Phys. Rev. Lett. **68**, 2952 (1992).
[6] N. Osakabe, H. Kasai, T. Kodama, and A. Tonomura, Phys. Rev. Lett. **78**, 1711 (1997).
[7] N. Osakabe, K. Harada, M. I. Lutwyche, H. Kasai, and A. Tonomura, Appl. Phys. Lett. **70**, 940 (1997).
[8] N. Osakabe, T. Kodama, J. Endo, A. Tonomura, K. Ohbayashi, T. Urakami, S. Ohsuka, H. Tsuchiya, and Y. Tsuchiya, Nucl. Instrum. Methods Phys. Res. A **365**, 585 (1995).
[9] O. Bostanjoglo and R. Liedtke, Phys. Status Solidi A **60**, 451 (1980); O. Bostanjoglo and G. Schlotzhauer, *ibid.* **68**, 555 (1981); O. Bostanjoglo, *ibid.* **76**, 525 (1983).
[10] G. F. Knoll, *Radiation Detection and Measurement*, 2nd ed. (Wiley, New York, 1989).
[11] E. M. Purcell, Nature (London) **178**, 1449 (1956).
[12] O. Bostanjoglo, G. Schlotzhauer, and S. Schade, Optik (Stuttgart) **61**, 91 (1982).
[13] P. W. Hawkes and E. Kasper, *Principles of Electron Optics* (Academic, London, 1989), Vol. 2.
[14] K. Harada, T. Matsuda, J. Bonevich, M. Igarashi, S. Kondo, G. Pozzi, U. Kawabe, and A. Tonomura, Nature (London) **350**, 51 (1992).
[15] J. C. H. Spence, *Experimental High Resolution Electron Microscopy* (Oxford University Press, Oxford, 1980).
[16] A. Migliori, G. Pozzi, and A. Tonomura, Ultramicroscopy **49**, 87 (1993).
[17] T. Kawasaki, J. Endo, T. Matsuda, and A. Tonomura, Microbeam Anal. **3**, 287 (1994).
[18] G. Möllenstedt and H. Düker, Naturwissenschaften **42**, 41 (1955).
[19] A. Tonomura, *Electron Holography*, Vol. 70 of Springer Series in Optical Sciences, edited by K. Shimoda (Springer, Berlin, 1993).
[20] N. Osakabe, T. Urakami, T. Kodama, S. Ohsuka, H. Tsuchiya, Y. Tsuchiya, J. Endo, and A. Tonomura (unpublished).
[21] M. J. Berger, S. M. Seltzer, S. E. Chappell, J. C. Humphreys, and J. W. Motz, Nucl. Instrum. Methods **69**, 181 (1969).
[22] N. Osakabe, T. Kodama, T. Urakami, S. Ohsuka, H. Tsuchiya, Y. Tsuchiya, J. Endo, and A. Tonomura (unpublished).
[23] R. Asch and N. C. Ford, Rev. Sci. Instrum. **44**, 506 (1973); B. Chu, *Laser Light Scattering* (Academic, Orlando, 1974).
[24] K. Ohbayashi, Jpn. J. Appl. Phys. **13**, 1219 (1974).
[25] See, e.g., J. N. Butler and D. R. Quarrie, Phys. Today **49** (10), 50 (1996).
[26] *Semiconductors and Semimetals*, edited by W. T. Tsang (Academic, Orlando, 1985), Vol. 22, Part D.
[27] T. Kodama, N. Osakabe, J. Endo, A. Tonomura, K. Ohbayashi, T. Urakami, S. Ohsuka, H. Tsuchiya, Y. Tsuchiya, and Y. Uchikawa (unpublished).
[28] M. J. Buckingham, *Noise in Electronic Devices and Systems* (Wiley, New York, 1983).
[29] L. W. Swanson and A. E. Bell, in *Advances in Electronics and Electron Physics*, edited by L. Marton (Academic, New York, 1973) Vol. 32, p. 193.
[30] M. P. Silverman, Nuovo Cimento B **97**, 200 (1987).
[31] M. Born and E. Wolf, *Principles of Optics* (Pergamon, New York, 1959).
[32] R. Humbury-Brown and R. Q. Twiss, Nature (London) **177**, 27 (1956).
[33] T. Kodama, N. Osakabe, J. Endo, A. Tonomura, K. Ohbayashi, T. Urakami, S. Ohsuka, H. Tsuchiya, Y. Tsuchiya, and Y. Uchikawa (unpublished).
[34] M. P. Silverman, Phys. Lett. A **118**, 155 (1986); **122**, 226 (1987); **148**, 154 (1990).
[35] T. Matsuda, K. Harada, H. Kasai, O. Kamimura, and A. Tonomura, Science **271**, 1393 (1996); K. Harada, O. Kamimura, H. Kasai, T. Matsuda, A. Tonomura, and V. V. Moshchalkov, *ibid.* **274**, 1167 (1996).
[36] J. E. Bonevich, K. Harada, H. Kasai, T. Matsuda, T. Yoshida, G. Pozzi, and A. Tonomura, Phys. Rev. B **49**, 6800 (1994).
[37] See, e.g., H. J. Jensen, A. Brass, and A. Berlinsky, Phys. Rev. Lett. **60**, 1676 (1988); U. Yaron, P. L. Gammel, D. A. Huse, R. N. Kleiman, C. S. Oglesby, E. Bucher, B. Batlogg, D. J. Bishop, K. Mortensen, and K. N. Clausen, Nature (London) **376**, 753 (1995); S. N. Gordeev, P. A. J. de Groot, M. Oussena, A. V. Volkozub, S. Pinfold, R. Langan, R. Gagnon, and L. Taillefer, *ibid.* **385**, 324 (1997).
[38] R. M. Fleming and C. C. Grimes, Phys. Rev. Lett. **42**, 1423 (1979); J. Dumas, C. Schlenker, J. Marcus, and R. Buder, *ibid.* **50**, 757 (1983); G. Grüner and A. Zettl, Phys. Rep. **119**, 117 (1985).
[39] An early review is found in J. R. Clem, Phys. Rep. **75**, 1 (1981)
[40] T. W. Ebbesen, Phys. Today **49** (6), 26 (1996).
[41] T. Tiedje, R. R. Haering, and W. N. Hardy, J. Acoust. Soc. Am. **65**, 1171 (1979).
[42] M. M. J. Treacy, T. W. Ebbesen, and J. M. Gibson, Nature (London) **381**, 678 (1996).
[43] Y. Martin and H. K. Wickramasinghe, Appl. Phys. Lett. **50**, 1455 (1987).
[44] B. Yurke, Phys. Rev. Lett. **56**, 1515 (1986); M. P. Silverman, Phys. Lett. A **124**, 27 (1987); M. Kitagawa and M. Ueda, Phys. Rev. Lett. **67**, 1852 (1991); M. Ban, Phys. Rev. A **49**, 4142 (1994).